Electronic Supplementary Information

Molecular Engineering of Colorless, Extremely Tough, Superiorly Self-Recoverable, and Healable Poly(Urethane-Urea) Elastomer for Impact-Resistant Applications

Dong Wang,[a] ZhiFeng Wang,[b] ShangYang Ren,[a] JianHua Xu,[a] Cheng Wang,[a] Po Hu,[a] and JiaJun Fu*[a]

[a]School of Chemical Engineering, Nanjing University of Science and Technology, Nanjing 210094, P. R. China
[b]Testing Center, Yangzhou University, Yangzhou 225002, P. R. China
*Corresponding Author: fujiajun668@gmail.com (J. J. Fu)

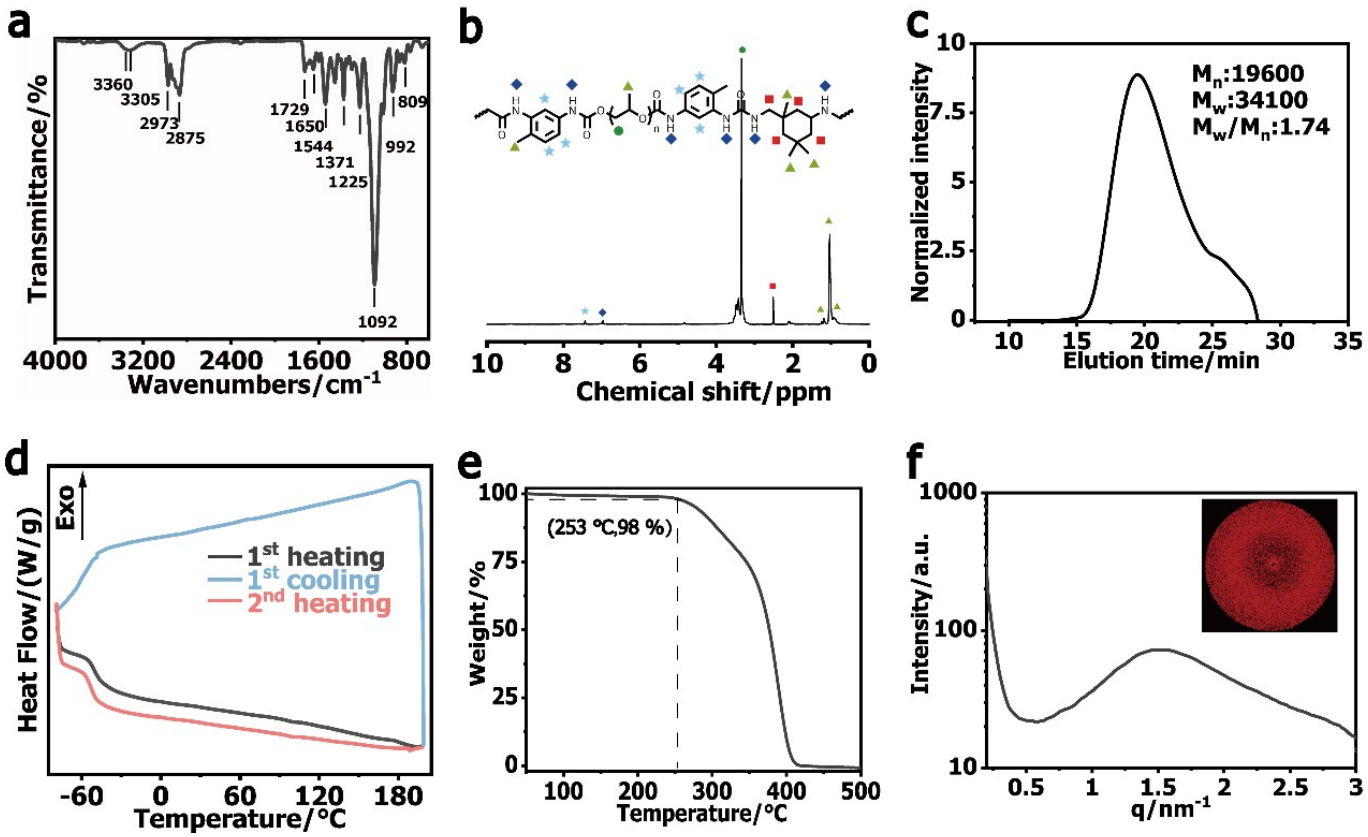

Fig. S1 Characterization of PPGTD-IPDA. a) FTIR of PPGTD-IPDA. FTIR (cm^{-1}): 3360/3305 (ν_{-NH-}), 2875/2973 (ν_{-CH_3}), 1371 (δ_{-CH_3}), 1729 ($\nu_{C=O}$, urethane), 1650 ($\nu_{C=O}$, urea), 1544 (γ_{-NH-}), 992/809 ($\delta_{-C_7H_6-}$), 1225 (ν_{-C-C-}), and 1092 ($\nu_{-C-O-C-}$). b) ^{1}H NMR of PPGTD-IPDA (500 MHz, $(CD_3)_2SO$, 25 °C). c) GPC elution curve of PPGTD-IPDA. d) DSC curve of PPGTD-IPDA. Neither endothermic nor exothermic peak was found, indicating the amorphous state. e) TGA curve of PPGTD-IPDA. No obvious degradation before 250 °C indicates its thermal-stability. f) SAXS data of PPGTD-IPDA. The microphase-separated structure was identified.

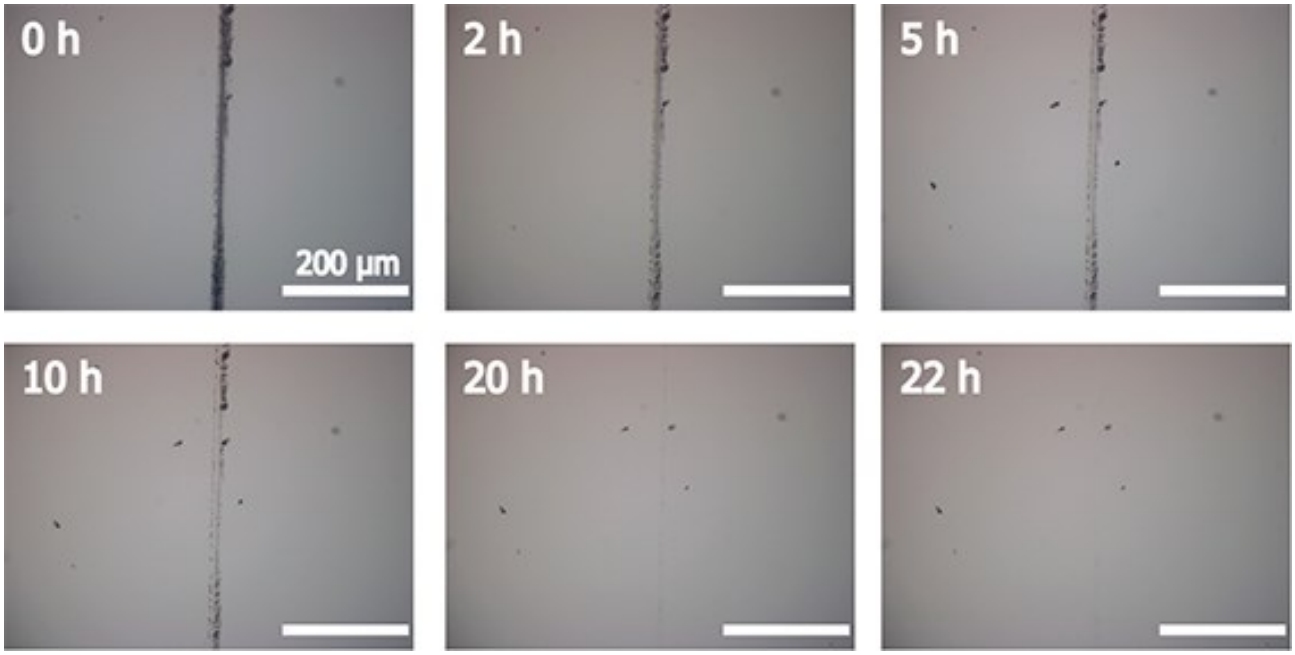

Fig. S2 Optical microscopy images of artificial scratch on the PPGTD-IPDA specimen before and healing for different time under ambient conditions.

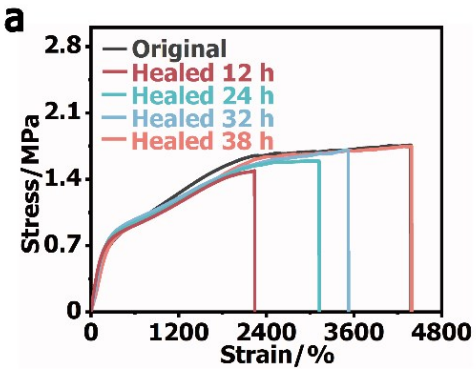

b

Healed time	Toughness (MJ m^{-3})	Elongation at break(%)	Healing efficiency(%)
Original	57.6	4379	/
Healed 12 h	24.4	2238	42.4
Healed 24 h	38.8	3122	67.4
Healed 32 h	46.4	3522	80.5
Healed 38 h	56.2	4388	97.6

Fig. S3 a) Tensile stress–strain curves of PPGTD-IPDA specimens at different healing time under ambient conditions. b) Summary of mechanical properties of PPGTD-IPDA at different healing time. The healing efficiency is defined as the proportion of toughness restored relative to the original toughness (area under the stress-strain curve).

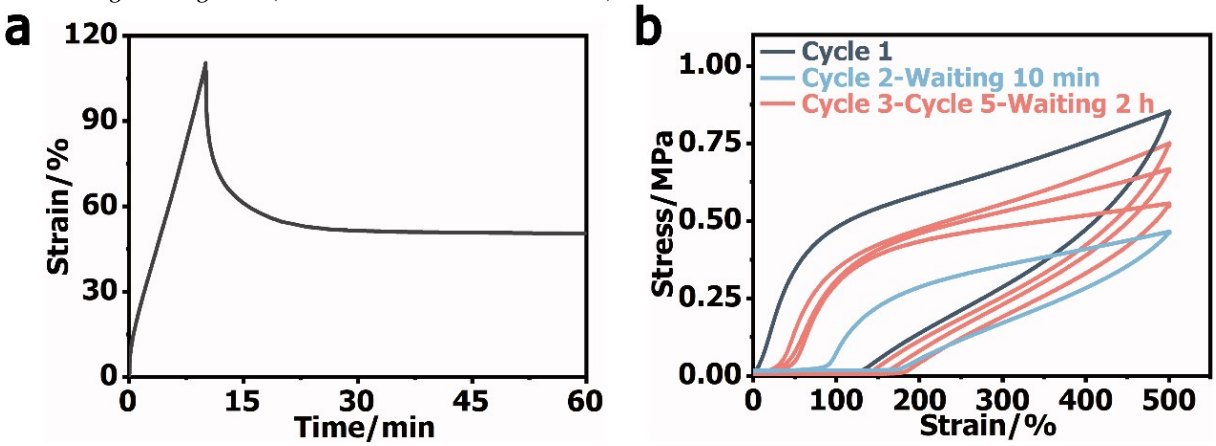

Fig. S4 a) Creep-recovery behavior of PPGTD-IPDA specimen at a stress of 0.08 MPa. The distinct residual strain was observed, meaning the noncovalent network could not return back to the original state. b) Cyclic tensile curves of PPGTD-IPDA specimen at a strain of 500%. As shown, the specimen could not eliminate the residual strain within 2 h after being stretched to 5× its original length.

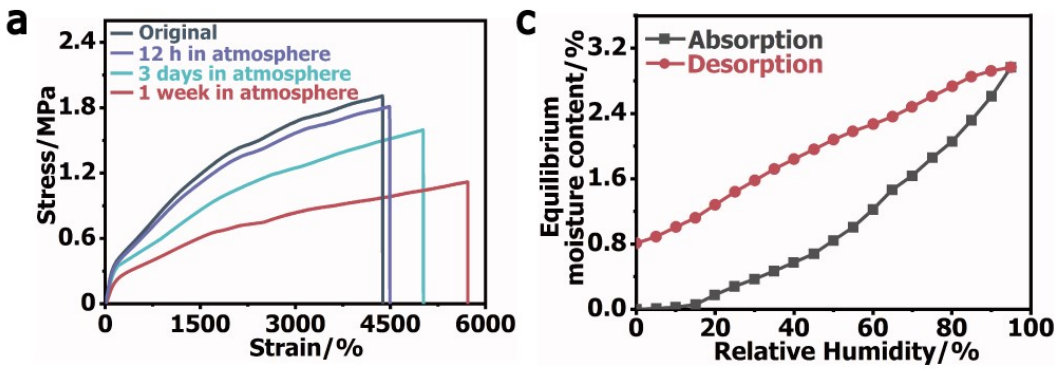

b

Sample	Original	12h in atmosphere	3 days in atmosphere	1 week in atmosphere
Young's modulus/MPa	0.34	0.32	0.26	0.16
Elongation at break/%	4380	4490	5010	5720
Tensile strength/MPa	1.90	1.82	1.60	1.12
Toughness/(MJ m^{-3})	57.6	56.1	53.2	43.3

Fig. S5 a) Tensile stress-strain curves of the original, three-days-aging and one-week-aging PPGTD-IPDA specimens**. b)** Summary of the mechanical properties of PPGTD-IPDA specimens that being exposed to the outdoor for different time. The Young's modulus and the tensile strength decreased and the strain at break increased with time, revealing the elastomer gradually turned to weak and soft. c) Water vapour adsorption-desorption isotherm for PPGTD-IPDA specimen. As shown, it can be inferred that the water retained in PPGTD-IPDA can dissociate the loosely packed hard domains, resulting the degradation of mechanical strength.

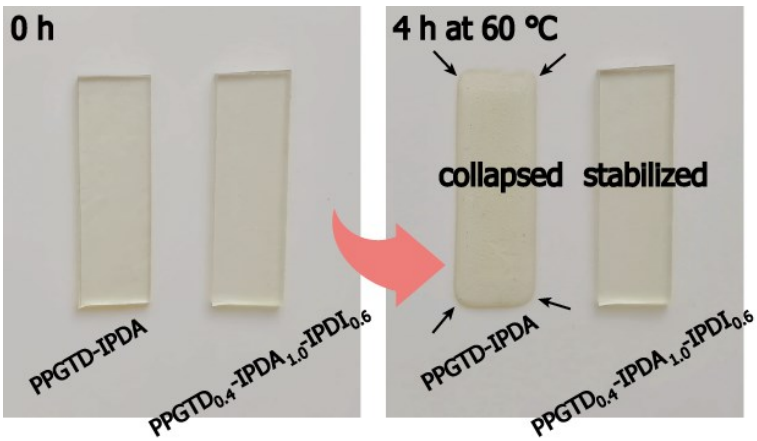

Fig. S6 Comparisons of PPGTD-IPDA and $PPGTD_{0.4}$-$IPDA_{1.0}$-$IPDI_{0.6}$ at 25 °C and 60 °C for 4 h for assessing the stability at relatively high temperature. As shown, $PPGTD_{0.4}$-$IPDA_{1.0}$-$IPDI_{0.6}$ was very stable after being heated. However, the four corners of PPGTD-IPDI were obviously collapsed, indicating the inferior thermal stability.

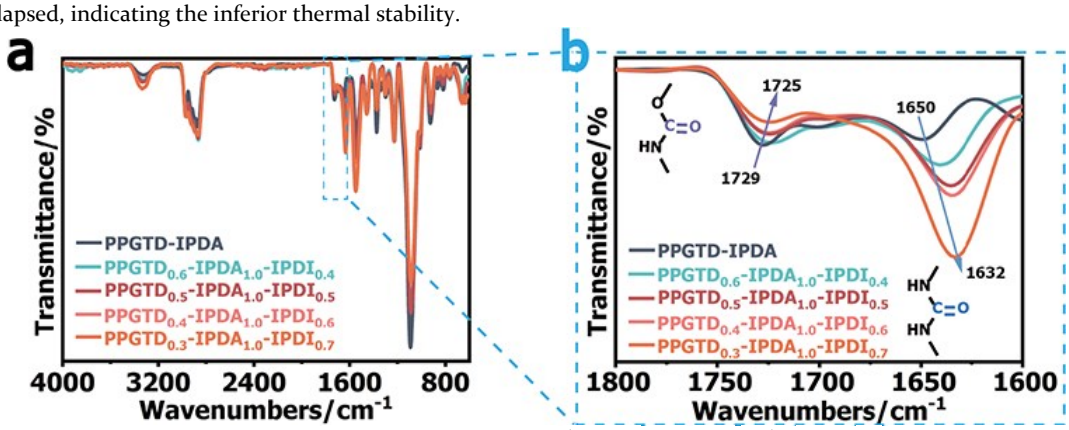

Fig. S7 FTIR spectra of PPGTD-IPDA and $PPGTD_{1-x}$-$IPDA_{1.0}$-$IPDI_x$ (X=0.4, 0.5, 0.6, 0.7). FTIR of $PPGTD_{0.4}$-$IPDA_{1.0}$-$IPDI_{0.6}$ (cm^{-1}): 3312/3362(ν_{-NH-}), 2875/2973 (ν_{-CH_3}), 1371 (δ_{-CH_3}), 1725($\nu_{C=O}$, urethane), 1632($\nu_{C=O}$, urea), 1544 (γ_{-NH-}), 992/809 ($\delta_{-C_7H_6-}$), 1225 (ν_{-C-C-}), and 1092 ($\nu_{-C-O-C-}$). As can be easily seen, with the increase of IPDI content, the intensity of $\nu_{C=O}$ at 1650 cm^{-1} (urea unit) increased, proving that the IPDI was covalently linked with IPDA in the hard domains. The intensity of $\nu_{C=O}$ at 1729 cm^{-1} (urethane unit), originating from PPGTD, accordingly decreased. In addition, the obvious shifts of $\nu_{C=O}$ confirm that the hard domains of $PPGTD_{1-x}$-$IPDA_{1.0}$-$IPDI_x$ assembled by H-bonds are different from PPGTD-IPDA.

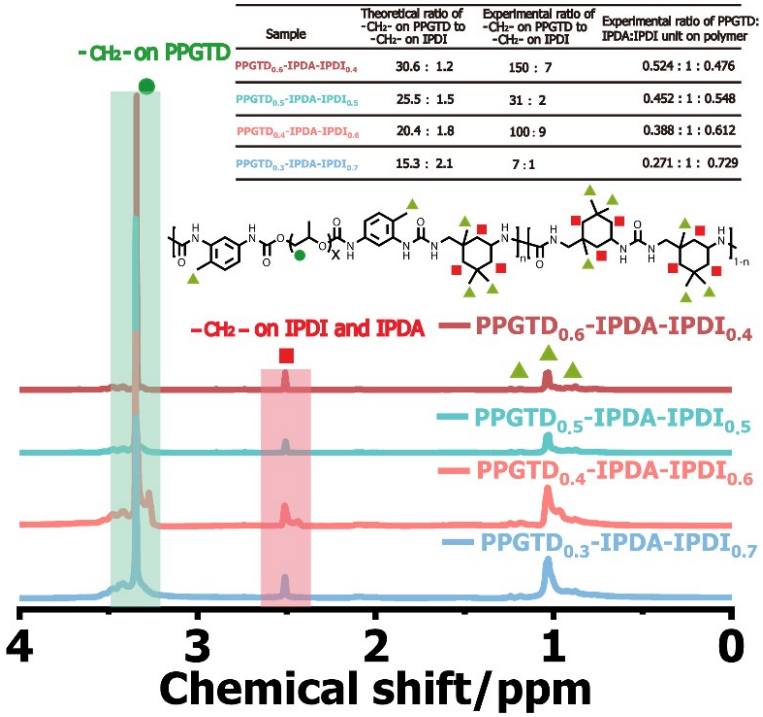

Sample	Theoretical ratio of -CH2- on PPGTD to -CH2- on IPDI	Experimental ratio of -CH2- on PPGTD to -CH2- on IPDI	Experimental ratio of PPGTD: IPDA:IPDI unit on polymer
$PPGTD_{0.6}$-IPDA-$IPDI_{0.4}$	30.6 : 1.2	150 : 7	0.524 : 1 : 0.476
$PPGTD_{0.5}$-IPDA-$IPDI_{0.5}$	25.5 : 1.5	31 : 2	0.452 : 1 : 0.548
$PPGTD_{0.4}$-IPDA-$IPDI_{0.6}$	20.4 : 1.8	100 : 9	0.388 : 1 : 0.612
$PPGTD_{0.3}$-IPDA-$IPDI_{0.7}$	15.3 : 2.1	7 : 1	0.271 : 1 : 0.729

Fig. S8 ^1H NMR of $PPGTD_{1-x}$-$IPDA_{1.0}$-$IPDI_x$ (x=0.4, 0.5, 0.6, 0.7), (500 MHz, $(CD_3)_2SO$, room temperature).

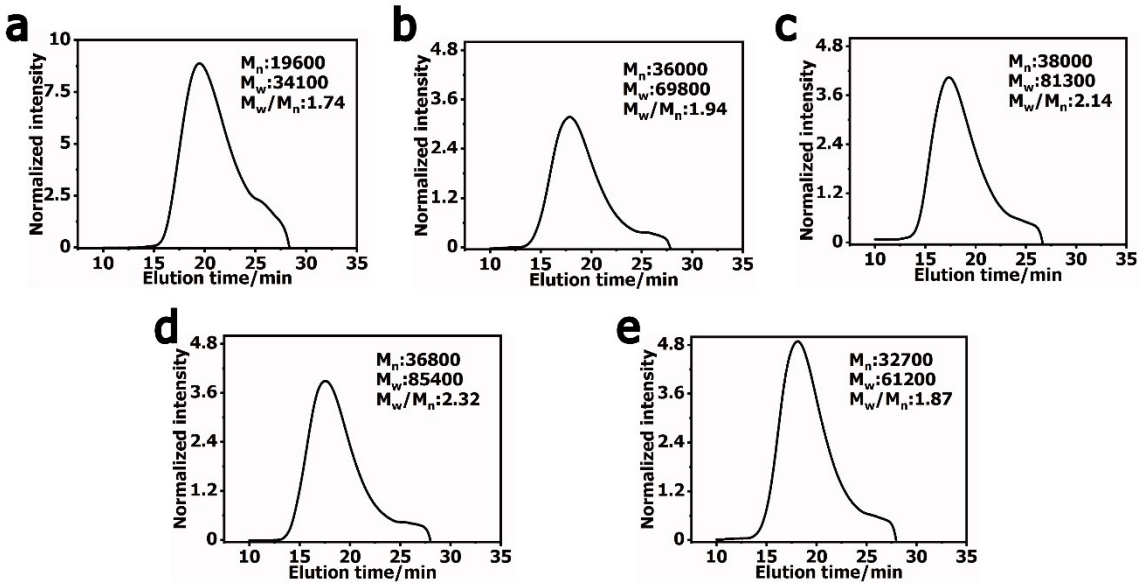

Fig. S9 GPC elution curves of a) PPGTD-IPDA, b) $PPGTD_{0.6}$-$IPDA_{1.0}$-$IPDI_{0.4}$, c) $PPGTD_{0.5}$-$IPDA_{1.0}$-$IPDI_{0.5}$, d) $PPGTD_{0.4}$-$IPDA_{1.0}$-$IPDI_{0.6}$, and e) $PPGTD_{0.3}$-$IPDA_{1.0}$-$IPDI_{0.7}$.

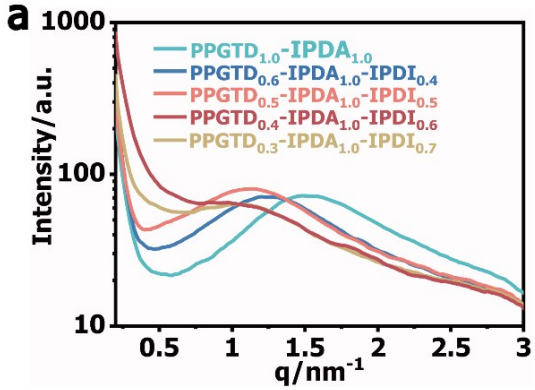

b

Sample	q/nm^{-1}	d/nm
PPGTD-IPDA	1.526	2.059
$PPGTD_{0.6}$-IPDA-$IPDI_{0.4}$	1.263	2.487
$PPGTD_{0.5}$-IPDA-$IPDI_{0.5}$	1.146	2.741
$PPGTD_{0.4}$-IPDA-$IPDI_{0.6}$	1.085	2.895
$PPGTD_{0.3}$-IPDA-$IPDI_{0.7}$	1.041	3.018

Fig. S10 a) SAXS data of $PPGTD_{1-x}$-$IPDA_{1.0}$-$IPDI_x$ specimens (x=0, 0.4, 0.5, 0.6, 0.7). b) Summary of the relative *q* vector and phase spacing *d* values of $PPGTD_{1-x}$-$IPDA_{1.0}$-$IPDI_x$.

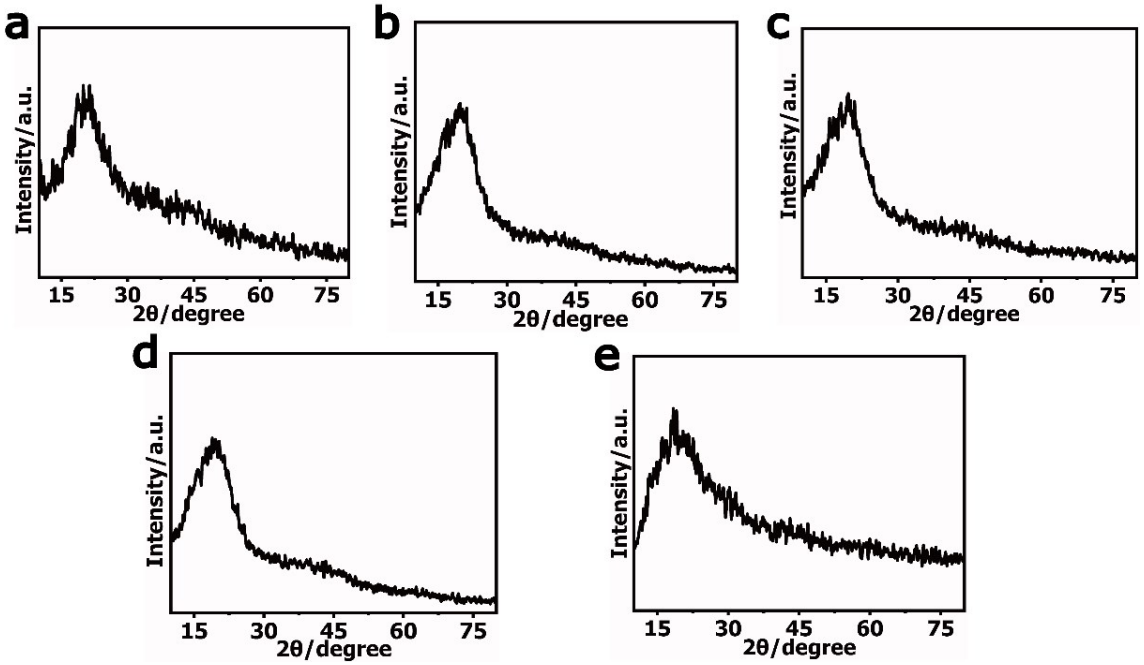

Fig. S11 XRD curves of $PPGTD_{1-x}$-$IPDA_{1.0}$-$IPDI_x$ (x=0.4, 0.5, 0.6, 0.7). As shown, all the curves only displayed a broad diffraction peak-centered, indicating the amorphous states under ambient conditions.

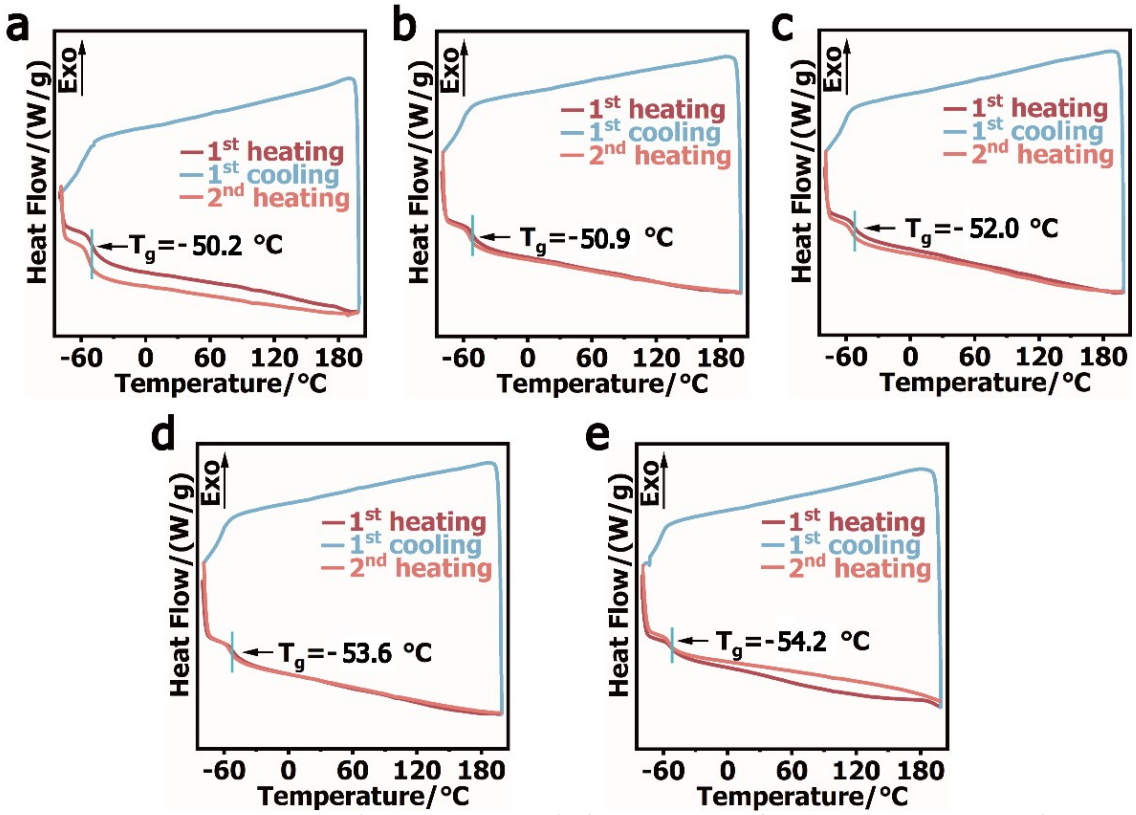

Fig. S12 DSC curves of $PPGTD_{1-x}$-$IPDA_{1.0}$-$IPDI_x$ (x=0,0.4, 0.5, 0.6, 0.7). a) PPGTD-IPDA, b) $PPGTD_{0.6}$-$IPDA_{1.0}$-$IPDI_{0.4}$, c) $PPGTD_{0.5}$-$IPDA_{1.0}$-$IPDI_{0.5}$, d) $PPGTD_{0.4}$-$IPDA_{1.0}$-$IPDI_{0.6}$, and e) $PPGTD_{0.3}$-$IPDA_{1.0}$-$IPDI_{0.7}$.

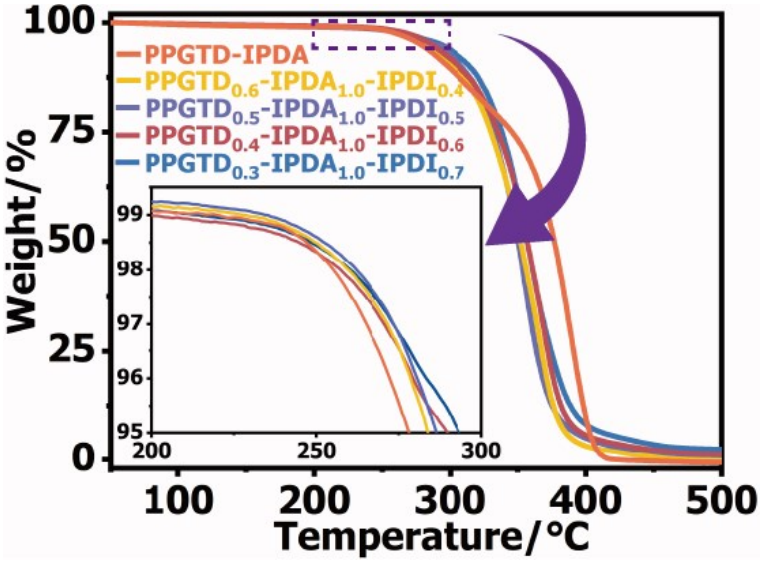

Fig. S13 TGA curve of $PPGTD_{1-x}$-$IPDA_{1.0}$-$IPDI_x$ (X=0.4, 0.5, 0.6, 0.7) upon heating from 50 to 500 °C at a rate of 10 °C min^{-1}.

Table S1 Summary of the mechanical properties of $PPGTD_{1-x}$-$IPDA_{1.0}$-$IPDI_x$ (x=0, 0.4, 0.5, 0.6, 0.7).

Sample	Strain at break(%)	Young's modulus(MPa)	Tensile strength(MPa)	Toughness (MJ m^{-3})
PPGTD-IPDA	4380	0.34	1.9	57.6
$PPGTD_{0.6}$-$IPDA_{1.0}$-$IPDI_{0.4}$	3740	3.5	19.9	392.5
$PPGTD_{0.5}$-$IPDA_{1.0}$-$IPDI_{0.5}$	3530	5.19	28.1	478.2
$PPGTD_{0.4}$-$IPDA_{1.0}$-$IPDI_{0.6}$	2970	7.84	33.4	503.3
$PPGTD_{0.3}$-$IPDA_{1.0}$-$IPDI_{0.7}$	1730	25.2	31.9	386.4

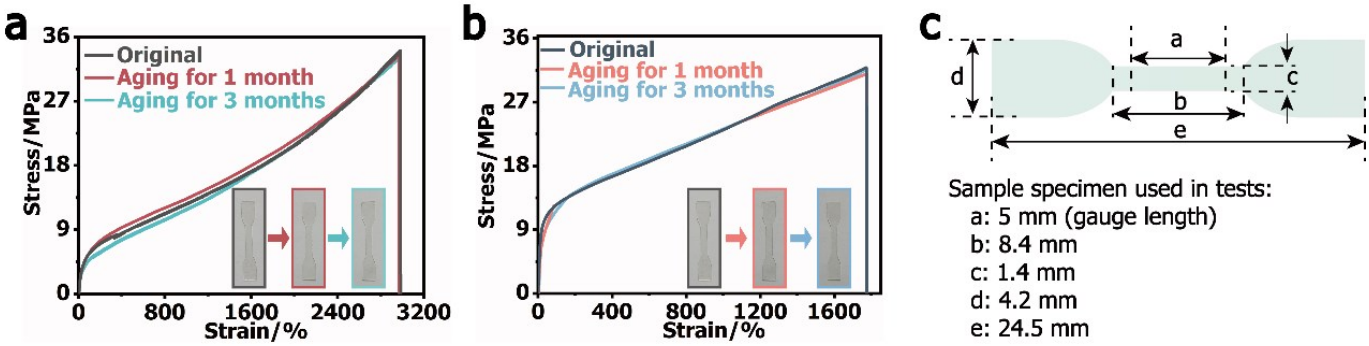

Fig. S14 The stress-strain curves for a) $PPGTD_{0.4}$-$IPDA_{1.0}$-$IPDI_{0.6}$ specimen and b) $PPGTD_{0.3}$-$IPDA_{1.0}$-$IPDI_{0.7}$ specimen obtained after being exposed to ambient conditions for 1 month and 3 months. c) Dimension illustration of dumbbell-shaped specimen.

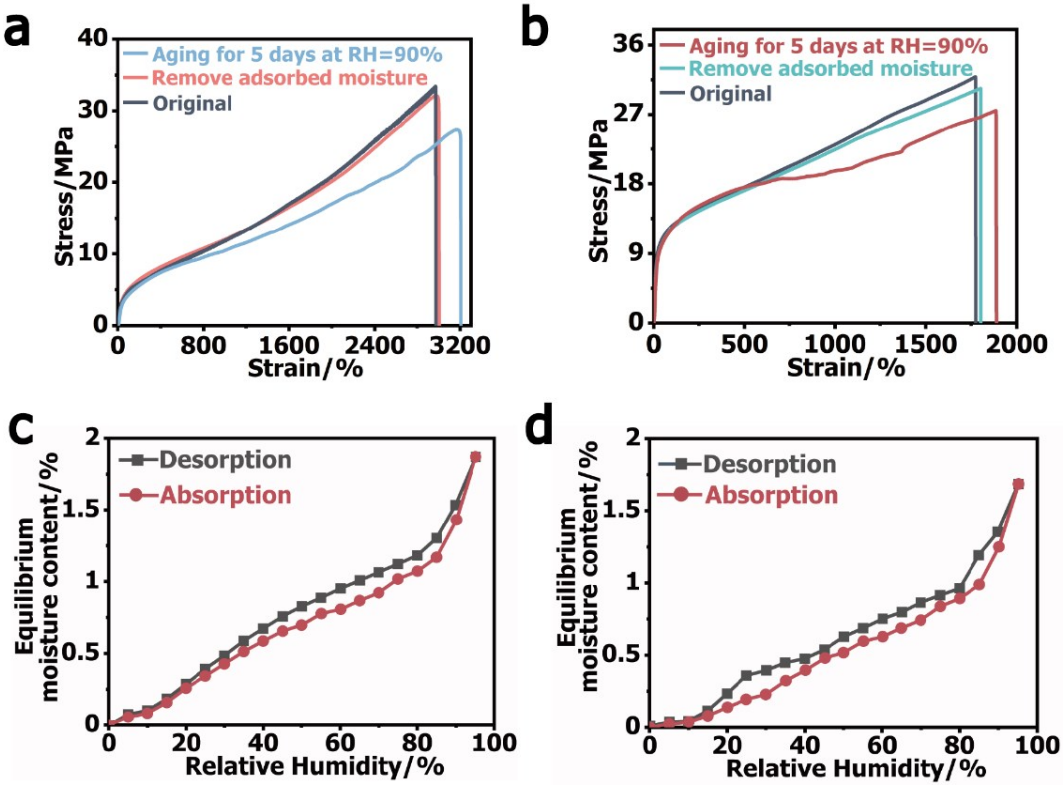

Fig. S15 a) $PPGTD_{0.4}$-$IPDA_{1.0}$-$IPDI_{0.6}$ and b) $PPGTD_{0.3}$-$IPDA_{1.0}$-$IPDI_{0.7}$ specimens were placed under high humidity at 25 °C. Water vapour adsorption-desorption isotherms for c) $PPGTD_{0.4}$-$IPDA_{1.0}$-$IPDI_{0.6}$ specimen and d) $PPGTD_{0.3}$-$IPDA_{1.0}$-$IPDI_{0.7}$ specimen. Measurements were performed at different relative humidity from RH = 0% to RH = 95% with an interval of 5%. After being placed under high humidity (RH=95%, Temp=25°C) for five days, the toughness of $PPGTD_{0.4}$-$IPDA_{1.0}$-$IPDI_{0.6}$ and $PPGTD_{0.3}$-$IPDA_{1.0}$-$IPDI_{0.7}$ only decreased from 503.3 and 386.4 MJ m^{-3} to 473.6 and 372.2 MJ m^{-3}, respectively. After removing the vapour, all the mechanical properties were all recovered to their original states.

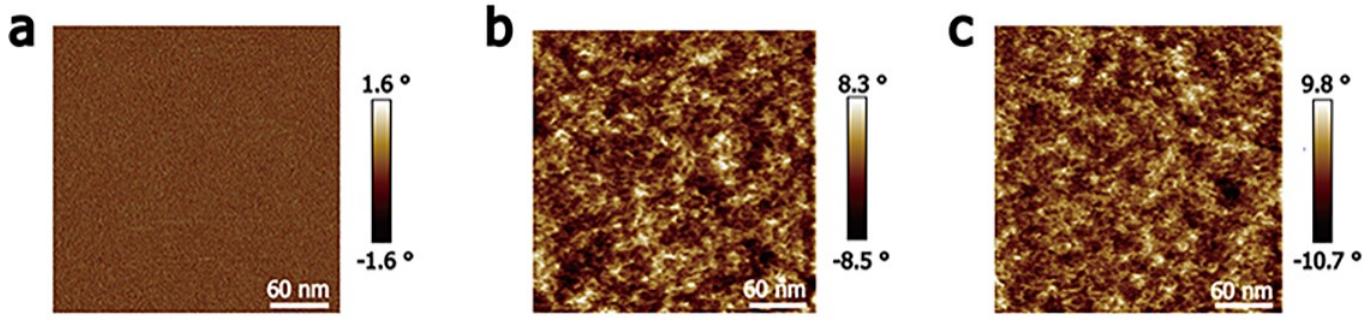

Fig. S16 AFM images of a) PPGTD-IPDA, b) $PPGTD_{0.4}$-$IPDA_{1.0}$-$IPDI_{0.6}$, and c) $PPGTD_{0.3}$-$IPDA_{1.0}$-$IPDI_{0.7}$. As shown, the microphase-separated structure became more and more visible with increasing IPDI content.

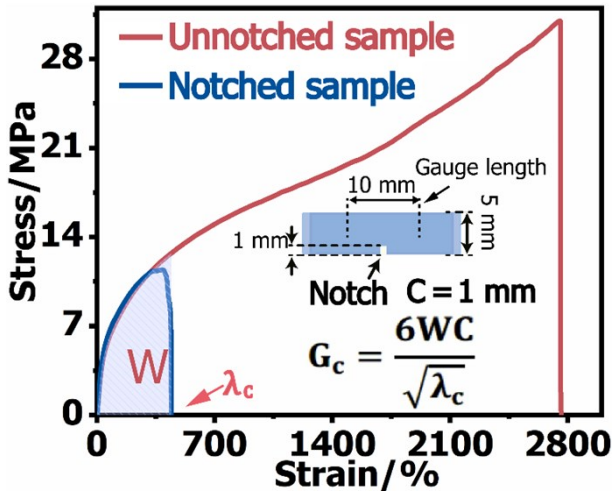

Fig. S17 Stress-strain of the unnotched and notched $PPGTD_{0.4}$-$IPDA_{1.0}$-$IPDI_{0.6}$ specimens (gauge length: 10 mm). A notch of 1 mm in length was artificially made on the one side of a rectangular specimen, and a deformation rate was 100 mm min^{-1}.

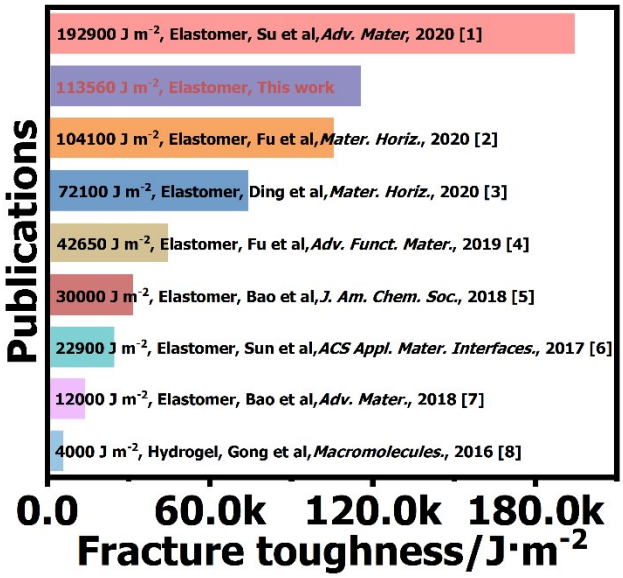

Fig. S18 Graphic comparison of fracture toughness for some tough elastomers and hydrogels reported in the previous literatures.

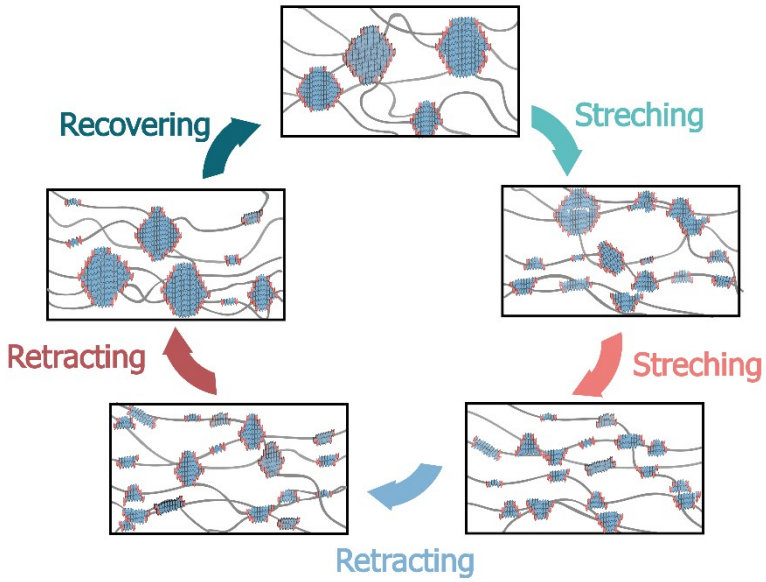

Scheme S1 Schematic illustrations of the evolution of hard domains during stretching-retracting process.

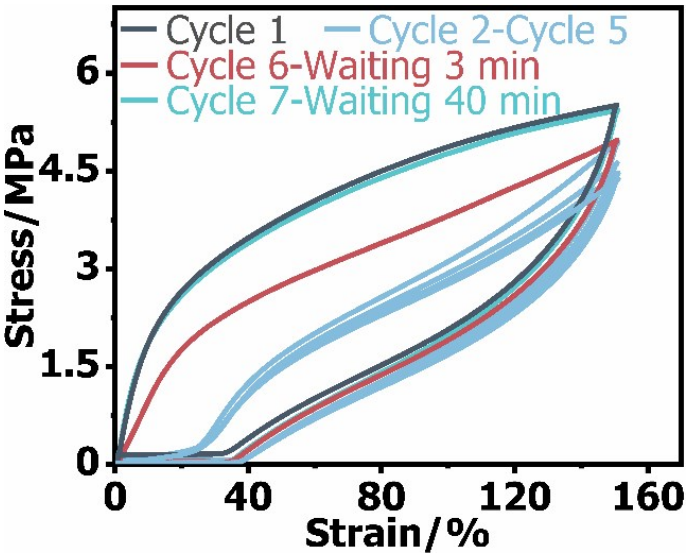

Fig. S19 Cyclic tensile curves of $PPGTD_{0.4}$-$IPDA_{1.0}$-$IPDI_{0.6}$ specimen at a strain of 150%. The specimen was loaded-unloaded without intervals between two consecutive cyclic tensile (cycle 1-cycle 5). After that, the specimen was allowed to relax for 3 min before the 6th cyclic tensile test to eliminate the residual strain. After 40 min resting, the energy dissipation ability was completely recovered.

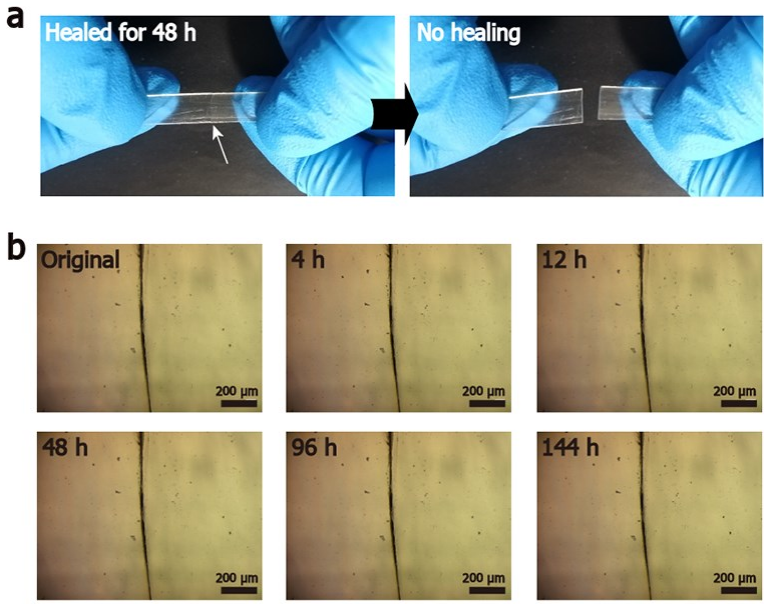

Fig. S20 No self-healing behavior of $PPGTD_{0.4}$-$IPDA_{1.0}$-$IPDI_{0.6}$ elastomer under ambient conditions. a) resplicing test and b) scratch test.

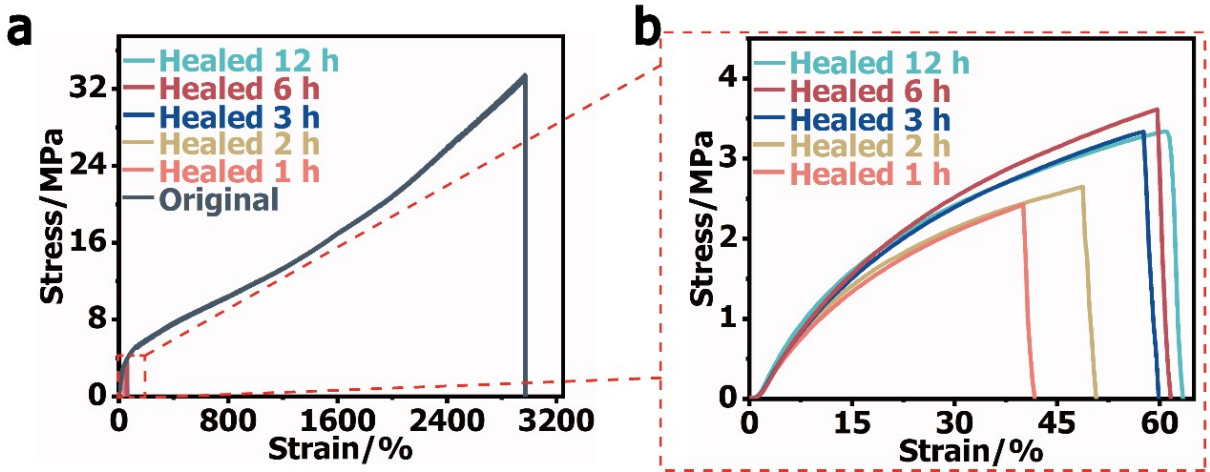

Fig. 21 Tensile stress-strain curves of $PPGTD_{0.4}$-$IPDA_{1.0}$-$IPDI_{0.6}$ specimens at different healing time under 80 °C. The right image enlarges the local region (strain: 0-60%) in the left image to clearly illustrate the low healing efficiency under relatively high temperature.

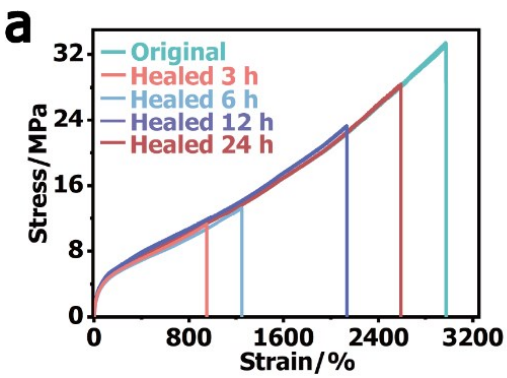

b

Healed time	Toughness (MJ m^{-3})	Elongation at break(%)	Healing efficiency(%)
Original	503.3	2970	/
Healed 3 h	70.6	947	14.0
Healed 6 h	104.1	1254	20.7
Healed 12 h	279.5	2138	55.5
Healed 24 h	386.5	2590	76.8

Fig. S22 a) Stress-strain curves of $PPGTD_{0.4}$-$IPDA_{1.0}$-$IPDI_{0.6}$ specimens healed under 140 °C with different healing time. b) Summary of mechanical properties of $PPGTD_{0.4}$-$IPDA_{1.0}$-$IPDI_{0.6}$ specimens with different healing time.

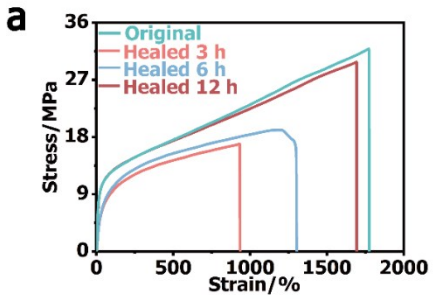

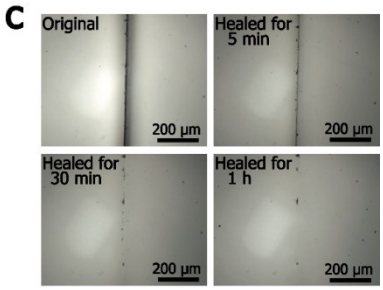

b

Healed time	Toughness (MJ m^{-3})	Elongation at break(%)	Healing efficiency(%)
Original	386.4	1730	/
Healed 2 h	124.3	932	32.2
Healed 6 h	201.2	1300	52.1
Healed 12 h	352.3	1690	91.2

Fig. S23 a) The tensile stress–strain curves of $PPGTD_{0.3}$-$IPDA_{1.0}$-$IPDI_{0.7}$ specimens at different healing time with the assistance of trace amount of DMF under ambient conditions. b) Summary of mechanical properties of $PPGTD_{0.3}$-$IPDA_{1.0}$-$IPDI_{0.7}$ at different healing time. c) Optical photographs showing the elimination of scratch on surface of $PPGTD_{0.3}$-$IPDA_{1.0}$-$IPDI_{0.7}$ specimen with the assistance of tiny DMF.

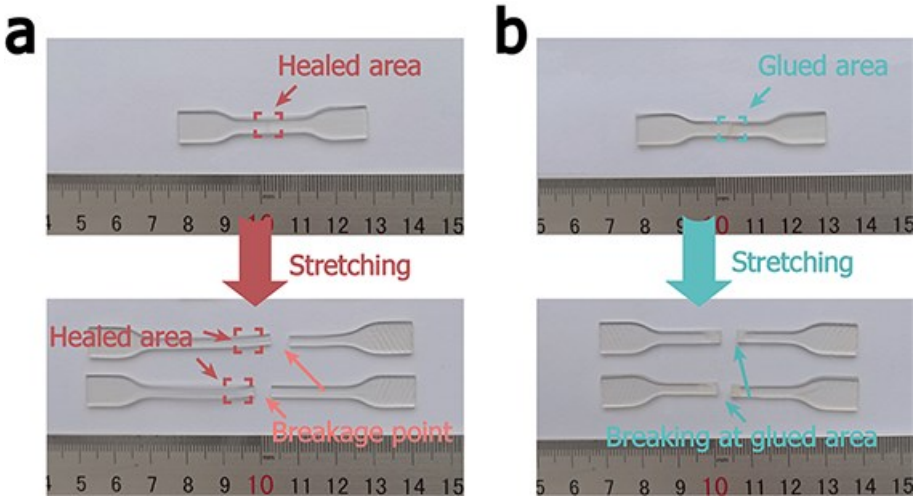

Fig. S24 a) Photographs for the healed $PPGTD_{0.4}$-$IPDA_{1.0}$-$IPDI_{0.6}$ from trace solvent-induced healing approach and the broken of the healed $PPGTD_{0.4}$-$IPDA_{1.0}$-$IPDI_{0.6}$ during stretching. b) Photographs for the glued $PPGTD_{0.4}$-$IPDA_{1.0}$-$IPDI_{0.6}$ from solvent-induced local dissolution approach and the broken of the glued $PPGTD_{0.4}$-$IPDA_{1.0}$-$IPDI_{0.6}$ during stretching.

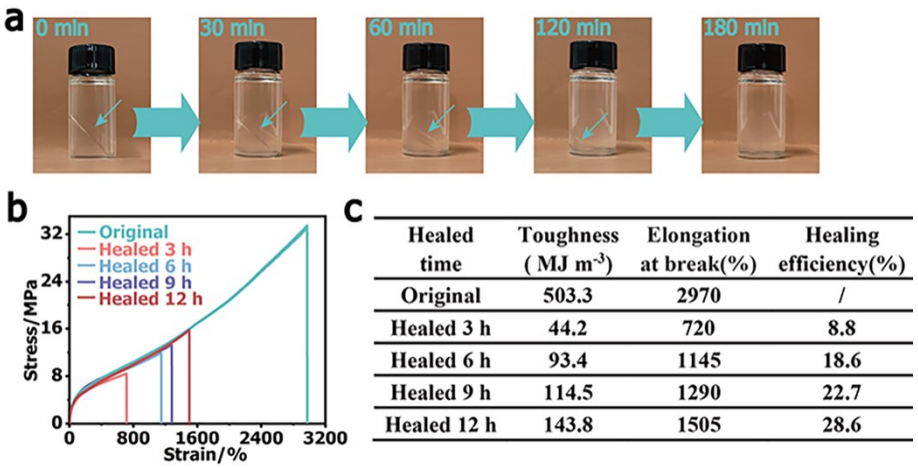

c

Healed time	Toughness (MJ m^{-3})	Elongation at break(%)	Healing efficiency(%)
Original	503.3	2970	/
Healed 3 h	44.2	720	8.8
Healed 6 h	93.4	1145	18.6
Healed 9 h	114.5	1290	22.7
Healed 12 h	143.8	1505	28.6

Fig. S25 a) Photographs for demonstrating the dissolution process of $PPGTD_{0.4}$-$IPDA_{1.0}$-$IPDI_{0.6}$ in n-BuOH. b) Stress-strain curves of the healed $PPGTD_{0.4}$-$IPDA_{1.0}$-$IPDI_{0.6}$ via trace n-BuOH-induced healing with different healing time. c) Summary of mechanical properties and healing efficiencies of the healed $PPGTD_{0.4}$-$IPDA_{1.0}$-$IPDI_{0.6}$. It can be clearly seen that although the specimen was dissolved in n-BuOH, the trace amount of n-BuOH could not achieve satisfactory healing efficiency. This result evidences that the dissolution effect is not mainly responsible for high healing efficiency.

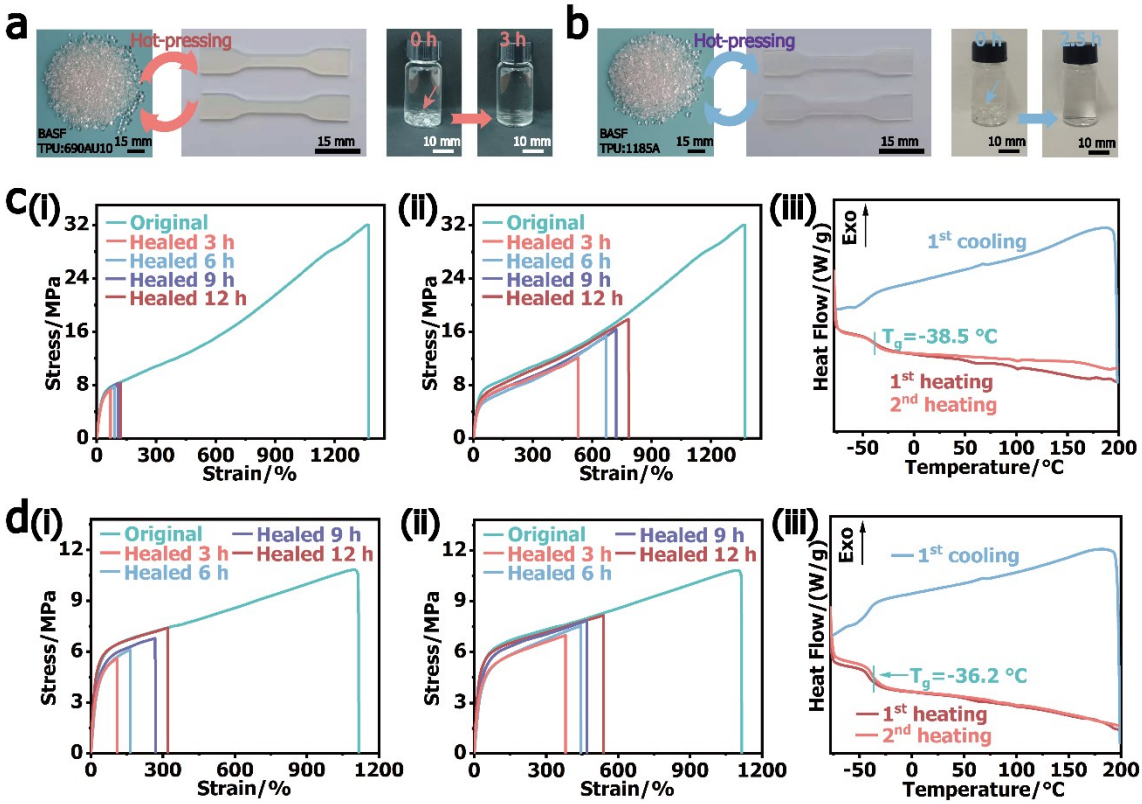

Fig. S26 Photographs of commercially available a) TPU 690AU10 and b) TPU 1185A purchased from BASF Co., Ltd. (China). These two thermoplastic polyurethanes were molded into dumbbell-shaped specimens via hot-pressing method. They are well dissolved in DMF. c) Stress-strain curves of the healed TPU 690AU10 specimens with different healing time from ⅰ) trace DMF-induced healing approach and ⅱ) DMF-induced local dissolution approach; ⅲ) DSC curves of TPU 690AU10. d) Stress-strain curves of the healed TPU 1185A specimens with different healing time ⅰ) trace DMF-induced healing approach and ⅱ) DMF-induced local dissolution approach; ⅲ) DSC curves of TPU 1185A.

Two thermoplastic polyurethanes, TPU 690AU10 and TPU 1184A were purchased from BASF Co., Ltd. (China). After being molded into dumbbell-shaped specimens via hot-pressing method, the healing experiments were performed from different approaches. Although the T_g values of these polyurethanes were far below room temperature, the healing efficiencies of 690AU10 and 1164A from trace solvent-induced healing were only 3.1 wt% and 22 wt%, respectively after 12 h healing, confirming that not all the thermoplastic polyurethanes can achieve high healing efficiency via trace solvent-induced healing approach. Designing suitable structure for thermoplastic polyurethanes is of significance to high healing efficiency. The healing efficiencies of 690AU10 and 1164A from solvent-induced local dissolution increased to 36.9% and 39.7%, respectively. However, this process is not a real "healing" due to the obvious dimensional changes on glued areas, making polyurethanes unsafe for further use. Therefore, although trace solvent-induced healing is a promising method, it is not easy to achieve high healing efficiency. The selection of proper solvent and how to design suitable structures of thermoplastics should be primarily considered.

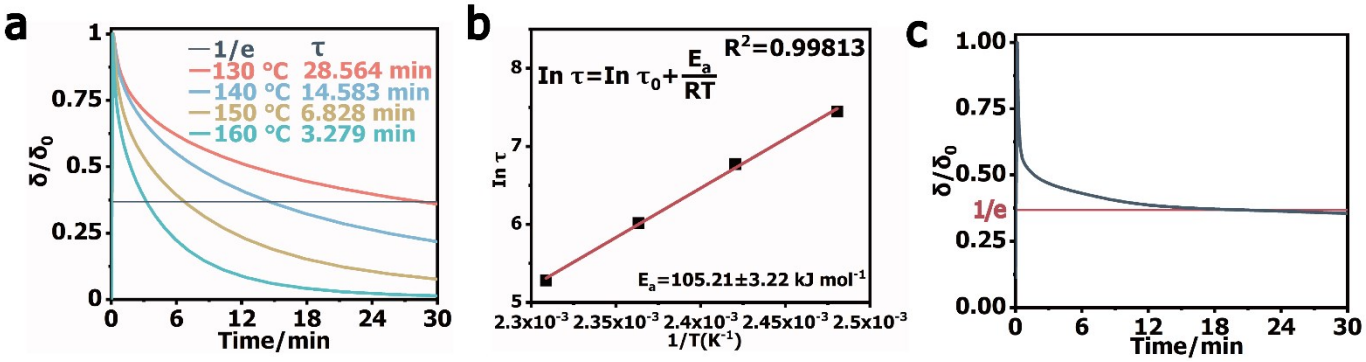

Fig. S27 a) Stress relaxation curves of $PPGTD_{0.4}$-$IPDA_{1.0}$-$IPDI_{0.6}$ specimens to 120% strain at different temperatures. b) ln τ - 1/T curve of $PPGTD_{0.4}$-$IPDA_{1.0}$-$IPDI_{0.6}$ specimen. As shown, the value of τ as a function of the inverse temperature follows Arrhenius' law, which is given by equation: $\ln \tau = \ln \tau_0 + E_a/RT$. The stress relaxation activation energy is calculated as 105.21 kJ mol^{-1} and the corresponding relaxation time (τ) at 25 °C is calculated as 1303 h. c) Stress relaxation curves of $PPGTD_{0.4}$-$IPDA_{1.0}$-$IPDI_{0.6}$ specimen absorbing DMF vapour in short time. As shown, the relaxation time (τ) dramatically decreased to 20.3 min, proving the solvent-accelerated exchange of H-bonds within hard domains.

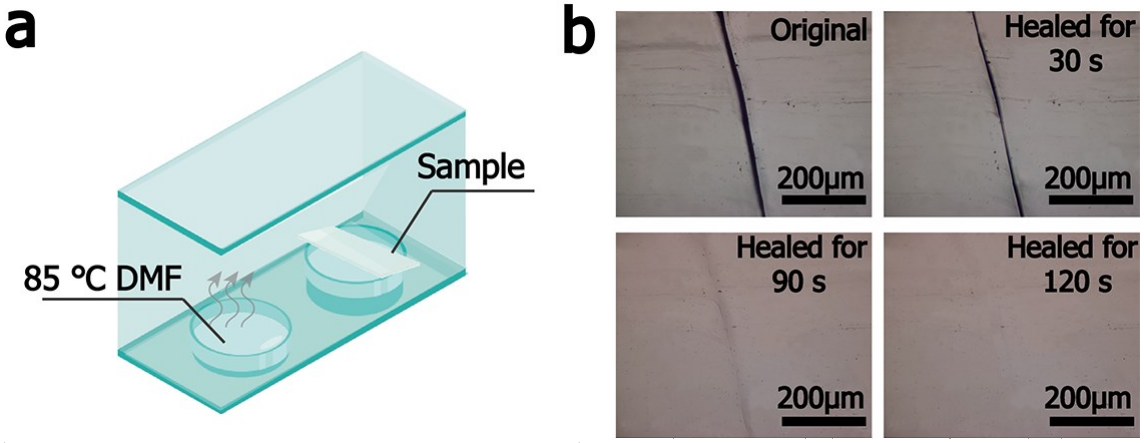

Fig. S28 a) Schematical illustration for healing in solvent vapour. b) Optical photographs of the surface scratch on $PPGTD_{0.4}$-$IPDA_{1.0}$-$IPDI_{0.6}$ film before and after healing in solvent vapour.

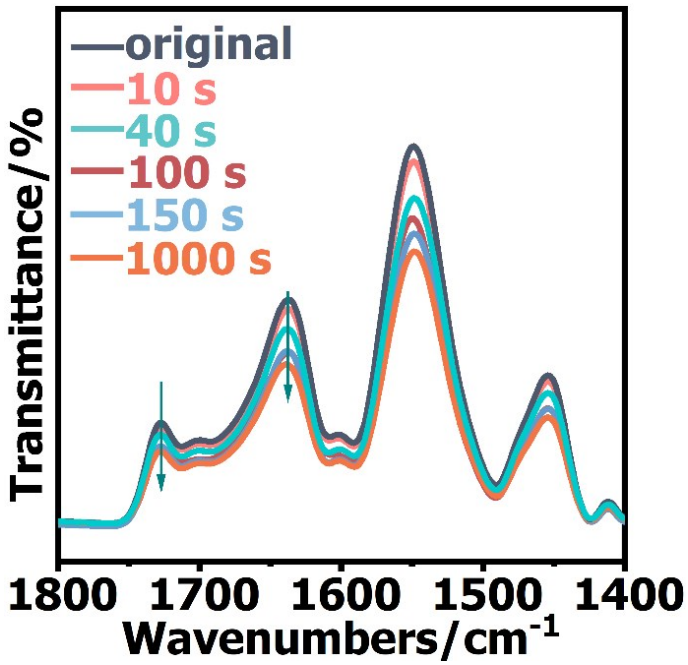

Fig. S29 Evolution of FTIR spectra of $PPGTD_{0.4}$-$IPDA_{1.0}$-$IPDI_{0.6}$ specimen that being contacted with trace n-BuOH. It can be clearly seen in Fig. S29, no obvious wavenumber shifts of $\nu_{C=O,\ urea}$ (1632 cm^{-1}) and $\nu_{C=O,\ urethane}$ (1726 cm^{-1}) were observed when trace n-BuOH was used. This is in sharp contrast to the trace DMF, indicating that the n-BuOH could not interfere the structure of H-bond and dissociate the hard domains in a short time.

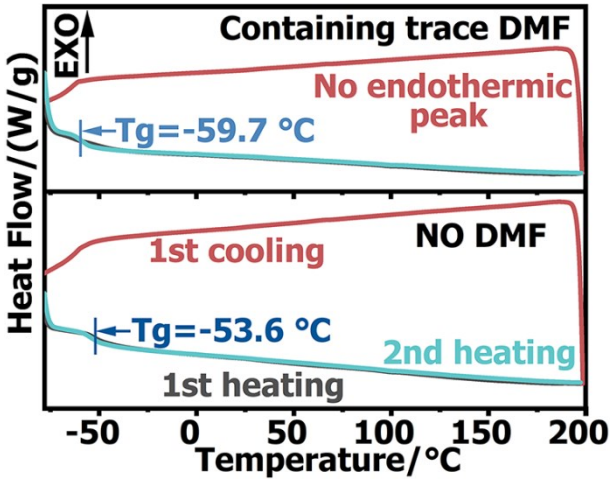

Fig. S30 DSC curves of $PPGTD_{0.4}$-$IPDA_{1.0}$-$IPDI_{0.6}$ without DMF and with the assitance of trace amount of DMF. As shown, DMF decreased T_g value from -53.6 to -59.7 °C, revealing that DMF could dissociate the hard domain and facilitate the mobility of polymeric chains.

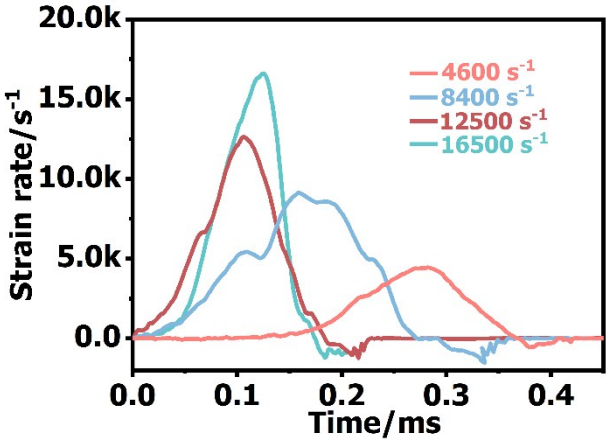

Fig. S31 Strain rate versus time in SHPB tests with different velocities at 25 °C.

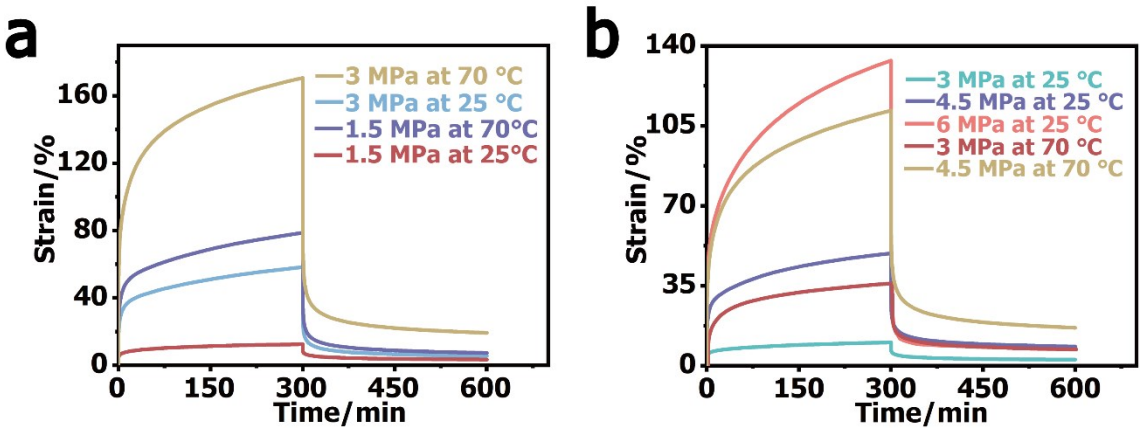

Fig. S32 Creep-recovery behaviors of a) $PPGTD_{0.4}$-$IPDA_{1.0}$-$IPDI_{0.6}$ specimen and b) $PPGTD_{0.3}$-$IPDA_{1.0}$-$IPDI_{0.7}$ specimen under different stress levels and temperatures. As shown, it is obvious that elevating temperature did not significantly change the creep-recovery behaviors of $PPGTD_{0.4}$-$IPDA_{1.0}$-$IPDI_{0.6}$, revealing the good thermal-resistance of IPDI-modified hard domains.

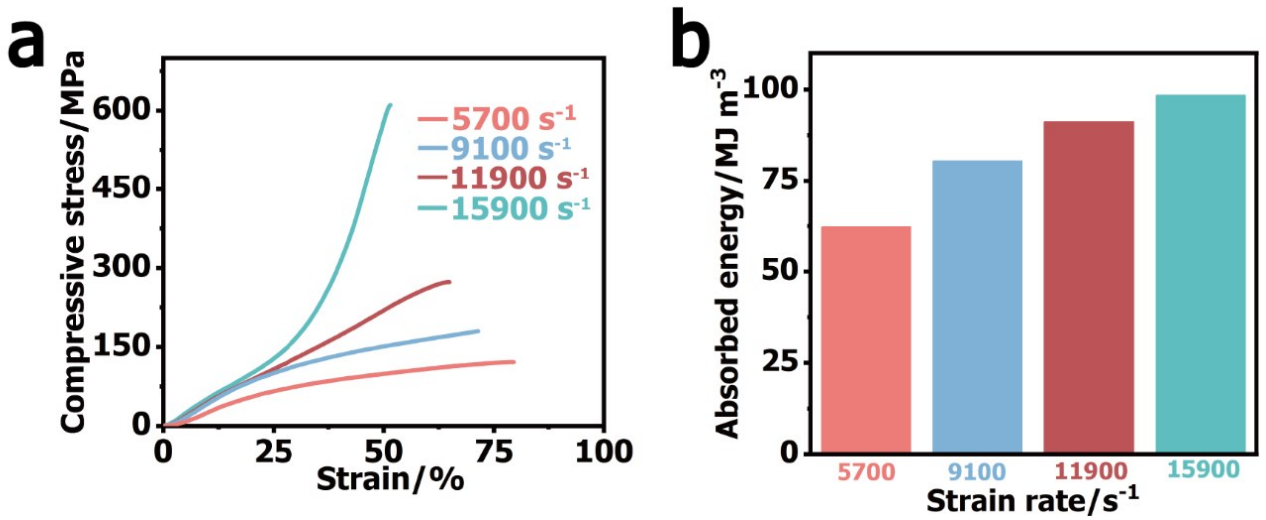

Fig. S33 a) Compressive stress-strain curves of $PPGTD_{0.3}$-$IPDA_{1.0}$-$IPDI_{0.7}$ specimen (diameter: 7 mm, thickness: 2 mm) for the SHPB tests with different strain rates. b) Effects of strain rates on absorbed energy.

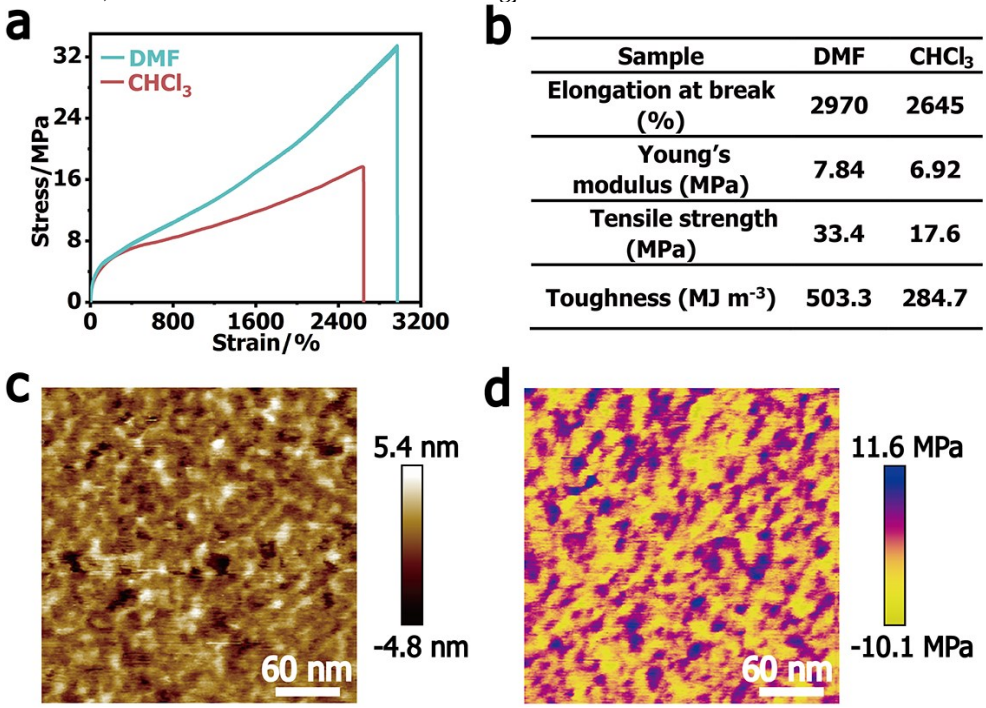

Sample	DMF	$CHCl_3$
Elongation at break (%)	2970	2645
Young's modulus (MPa)	7.84	6.92
Tensile strength (MPa)	33.4	17.6
Toughness (MJ m^{-3})	503.3	284.7

Fig. S34 a) Stress-strain curves of the $PPGTD_{0.6}$-$IPDA_{1.0}$-$IPDI_{0.4}$ using different solvents (DMF and $CHCl_3$). The synthetic procedures are the same except for solvents. b) Summary of mechanical properties of the $PPGTD_{0.6}$-$IPDA_{1.0}$-$IPDI_{0.4}$ obtained using DMF and $CHCl_3$ as solvent. AFM c) height and d) modulus map of a 300 × 300 nm^2 region of $PPGTD_{0.6}$-$IPDA_{1.0}$-$IPDI_{0.4}$ using $CHCl_3$ as solvent. As can be seen in Fig. S34, the mechanical properties of $PPGTD_{0.6}$-$IPDA_{1.0}$-$IPDI_{0.4}$ using $CHCl_3$ as solvent were inferior to that of $PPGTD_{0.6}$-$IPDA_{1.0}$-$IPDI_{0.4}$ using DMF as solvent. It can be inferred that difference of solvent polarity influences the composition of hard domains, including: binding mode/strength of H-bonds, altering the microstructure. Although $PPGTD_{0.6}$-$IPDA_{1.0}$-$IPDI_{0.4}$ using $CHCl_3$ as solvent retained microphase-separated structure, the modulus of hard domains was lower than that of $PPGTD_{0.6}$-$IPDA_{1.0}$-$IPDI_{0.4}$ using DMF as solvent, proving changes of the microstructure.

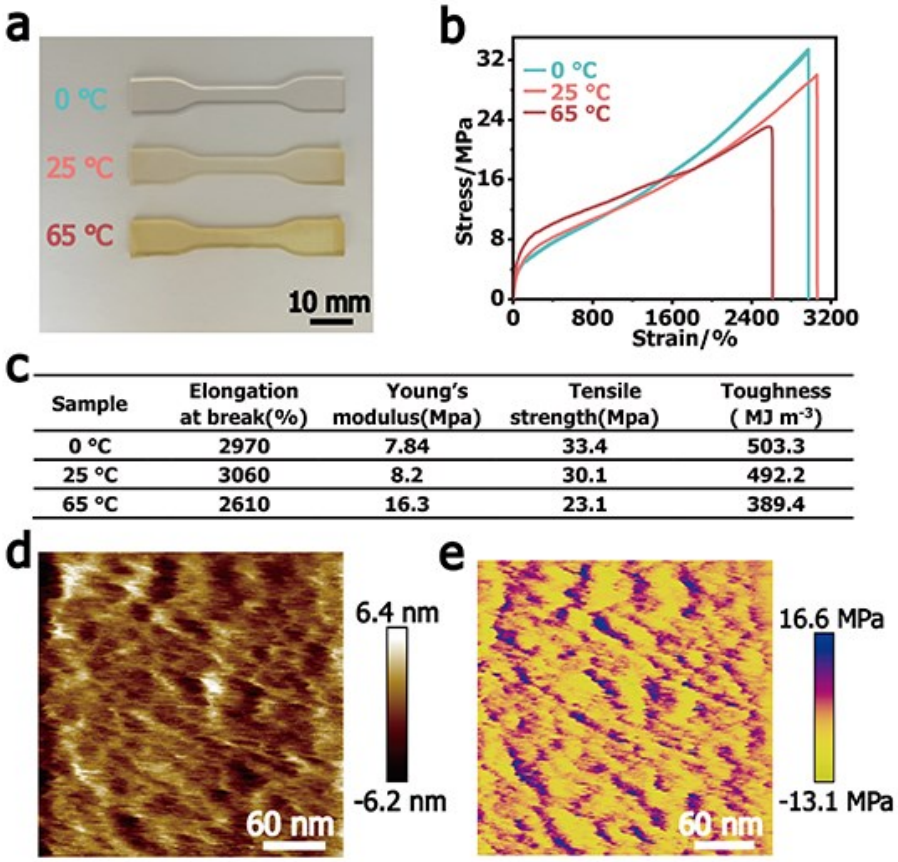

c

Sample	Elongation at break(%)	Young's modulus(Mpa)	Tensile strength(Mpa)	Toughness (MJ m^{-3})
0 °C	2970	7.84	33.4	503.3
25 °C	3060	8.2	30.1	492.2
65 °C	2610	16.3	23.1	389.4

Fig. S35 a) Dumbbell-shaped, b) Stress-strain curves, and c) Summary of mechanical properties of $PPGTD_{0.4}$-$IPDA_{1.0}$-$IPDI_{0.6}$ specimens obtained from different reaction temperatures. AFM d) height and e) modulus map of a 300 × 300 nm^2 region of $PPGTD_{0.4}$-$IPDA_{1.0}$-$IPDI_{0.6}$ obtained with the reaction temperature as 65 °C. As can be seen in Fig. S35, with the increase of the reaction temperature, the color of the specimens gradually turned from colorless to yellow. When the temperature was elevated to 65°C, the phenomenon of local gelation was observed. Although the high temperature accelerated the reaction rate and increased Young' modulus to a certain extent, the local gelation during reaction decreased the tensile strength and toughness. All properties considered, the optimal reaction temperature was determined as 0 °C.

References:

1. X. H. Wang, S. N. Zhan, Z. Y. Lu, J. Li, X. Yang, Y. N. Qiao, Y. F. Men, J. Q. Sun, *Adv. Mater.* **2020**, *32*, 2005759.
2. Y. H. Li, W. J. Li, A. L. Sun, M. F. Jing, X. J. Liu, L. H. Wei, K. Wu, Q. Fu, *Mater. Horiz.* **2021**, *8*, 267-275.
3. K. Song, W. J. Ye, X. C. Gao, H. G. Fang, Y. Q. Zhang, Q. Zhang, X. L. Li, S. Z. Yang, H. H. Wei, Y. S. Ding, *Mater. Horiz.* **2021**, *8*, 216-223.
4. D. Wang, J. H. Xu, J. Y. Chen, P. Hu, Y. Wang, W. Jiang, J. J. Fu, *Adv. Funct. Mater.* **2020**, *30*, 1907109.
5. X. Z. Yan, Z. Y. Liu, Q. H. Zhang, J. Lopez, H. Wang, H. C. Wu, S. M. Niu, H. P. Yan, S. H. Wang, T. Lei, J. H. Li, D. P Qi, P. G. Huang, J. P. Huang, Y. Zhang, Y. Y. Wang, G. L. Li, J. B.H. Tok, X. D. Chen, Z. N. Bao, *J. Am. Chem. Soc.* **2018**, *140*, 5280-5289.
6. Y. Wang, X. K. Liu, S. H. Li, T.Q. Li, Y. Song, Z. D. Li, W. K. Zhang, J. Q. Sun, *ACS Appl. Mater. Interfaces.* **2017**, *9*, 29120-29129.
7. J. H. Kang, D. H. Son, G. J. N. Wang, Y. X. Liu, J. Lopez, Y. Kim, J. Y. Oh, T. Katsumata, J. Mun, Y. J. Lee, L. H. Jin, J. B.H. Tok, Z. N. Bao, *Adv. Mater.* **2018**, *30*, 1706846.
8. A. B. Ihsan, T. L. Sun, T. Kurokawa, S. N. Karobi, T. Nakajima, T. Nonoyama, C. K. Roy, F. Luo, J. P. Gong, *Macromolecules* **2016**, *49*, 4245-4252.

Video S1: Demonstration of the mechanically robust $PPGTD_{0.4}$-$IPDA_{1.0}$-$IPDI_{0.6}$ elastomer.
Video S2: Demonstration of the energy-absorbing ability of $PPGTD_{0.4}$-$IPDA_{1.0}$-$IPDI_{0.6}$ elastomer during ball-dropping test.
Video S3: Demonstration of the rebound effect of $PPGTD_{0.4}$-$IPDA_{1.0}$-$IPDI_{0.6}$ elastomer during SHPB test.
Video S4: Demonstration of the original $PPGTD_{0.4}$-$IPDA_{1.0}$-$IPDI_{0.6}$ elastomer during drop hammer impact test.
Video S5: Demonstration of the recovered $PPGTD_{0.4}$-$IPDA_{1.0}$-$IPDI_{0.6}$ elastomer during drop hammer impact test.
Video S6: Demonstration of the damage of $PPGTD_{0.4}$-$IPDA_{1.0}$-$IPDI_{0.6}$ elastomer during drop hammer impact test.
Video S7: Demonstration of the healed $PPGTD_{0.4}$-$IPDA_{1.0}$-$IPDI_{0.6}$ elastomer during drop hammer impact test.